Accepted for publication in Composites Part: B

Published in September 12, 2012

DOI: 10.1016/j.compositesb.2012.09.013

Binary and ternary composites of polystyrene, styrene-butadiene rubber and boehmite produced by water-mediated melt compounding: Morphology and mechanical properties

S. Siengchin[1*] and J. Karger-Kocsis[2,3]

1- Production Engineering Department, The Sirindhorn International Thai-German Graduate School of Engineering (TGGS), King Mongkut's University of Technology North Bangkok, 1518 Pibulsongkram Road, Bangsue, Bangkok 10800, Thailand

2- Department of Polymer Engineering, Faculty of Mechanical Engineering, Budapest University of Technology and Economics, H-1111 Budapest, Hungary

3- MTA–BME Research Group for Composite Science and Technology, Muegyetem rkp. 3., H-1111 Budapest, Hungary

Submitted to Composite Part B, May and revised July 2012

* to whom correspondence should be addressed

(E-mail: suchart.s.pe@tggs-bangkok.org)

Tel. +66 2 913 2500 ext. 2920

Fax: +66 2 913 5805

Abstract

Binary and ternary composites composed of polystyrene (PS), styrene-butadiene rubber (SBR), and synthetic boehmite alumina (BA) were produced by water-mediated melt compounding technique. SBR latex and/or aqueous BA suspension was injected into the molten PS in a twin-screw extruder to prepare toughened and/or reinforced polymer composites. The dispersion of the BA (two fractions with different mean particle sizes) and SBR was studied by scanning- and transmission electron microcopy techniques (SEM and TEM, respectively), and discussed. The mechanical properties of the composites were determined in static tensile, Charpy impact and short-time stress relaxation tests (performed at various temperatures). It was found that BA was mostly embedded in the SBR phase in the ternary PS/SBR/BA composite. BA incorporation increased the stiffness and tensile strength and reduced the elongation at break and impact toughness. Effect of the BA particle size was most pronounced in the tensile mechanical and stress relaxation tests. Additional incorporation of BA in the PS/SBR blend enhanced the tensile modulus and stress relaxation modulus compared to the PS/SBR blend. Relaxation master curves were constructed by applying the time-temperature superposition (TTS) principle. It was established that the inverse of the Findley power law model was fairly applicable to the stress relaxation results.

Keywords: A. Processing technologies, B. Stress relaxation, D. Particle-reinforcement, E. Thermoplastic resin

1. INTRODUCTION

Polystyrene (PS) is one of the most widely used plastic materials. PS is often modified with nanoscale particles to improve the thermal and physical–mechanical properties [1-3] (e.g. thermal stability, stiffness, strength and creep resistance properties). Different nanoparticles, such as organophilic layered silicates [4-9], metal oxides [10-11], carbon nanotubes [12] and surface-coated magnesium carbonate [13] were already incorporated in PS matrix. However, though the modification of polystyrene with nanofillers results in enhanced strength and stiffness, it is usually accompanied with a loss in elongation at break and thus in toughness. Compounding with both rubber and rigid nanoparticles [14-15] has attracted considerable attention in R&D activities due to the promise of simultaneous improvements in stiffness and toughness characteristics of the corresponding polymeric composites. It was shown recently that the ternary composite composed of nanofiller/rubber/polyamide-6 (PA-6) and produced by water-mediated melt compounding (WM) outperformed the parent PA-6 with respect to fracture toughness [16]. We have also demonstrated on the example of polyoxymethylene (POM) that both toughening and reinforcing can be achieved on line using this compounding technique [17]. In the latter case, the boehmite alumina and polyurethane (PU) became nanoscale dispersed in the POM matrix. This allowed us to conclude that the WM technique is a proper tool to generate nanoscale dispersions. Moreover, the proposed water-mediated extrusion melt compounding is a very effective process being simple and cost-effective. Note that the expensive chemical modification of the nanofillers can be avoided provided that they are water swellable or dispersible.

The goal of this study was to explore the potential of the water mediated melt compounding technique to disperse boehmite alumina (BA) and styrene-butadiene rubber (SBR) in a polystyrene (PS) using a twin-screw extruder and compare the structure-property relationships of the resulting composites. The selection of the amorphous PS as matrix is reasoned by the fact that in its case changes in the crystalline morphology cause by the nanofiller and/or rubber additive can be excluded. SBR was selected as toughening agent for PS due to compatibility issue and introduced in the PS melt in form of a latex. BAs in two different mean particle sizes were used as nanofillers. The dispersion of BA and SBR in PS was assessed by scanning- and transmission electron microscopy techniques (SEM and TEM, respectively). The binary (PS/BA, PS/SBR) and ternary (PS/SBR/BA) nanocomposites were injection molded and the related specimens subjected to tensile, impact and short term stress relaxation tests at various temperatures.

2. EXPERIMENTAL

Materials and preparation of composites

Two types of water dispersible boehmite alumina (BA; AlO(OH); Disperal® P2 and Dispal®11N7-80 of Sasol GmbH, Hamburg, Germany) served as fillers. The nominal crystallite size of these BA grades (P2 and 11N7-80) was 4.5 and 30 nm, though that of the initial BA powders was 45 and 40 µm, respectively. P2 had an Al_2O_3 content of 72 wt.% and a specific surface area of 260 m^2/g whereas these values for 11N7-80 were 80 wt.% and 100 m^2/g. According to suppliers' information – bitte hier die Webseite angeben, the dispersed particle size of these P2 and 11N7-80 grades in 10 wt.% concentration in water was 25 and 220 nm, respectively. That is the reason why these BA grades will be referred to BA 25nm and BA 220nm, respectively, next. Styrene-butadiene rubber (SBR) latex with 40 wt.% dry content was kindly provided by Polymer Latex GmbH (Marl, Germany). Granulated PS

(Polystyrol 158 K Glasklar, BASF, Ludwigshafen, Germany) was utilized as a polymeric matrix for all the composite systems. The volumetric melt flow rate of PS (MVR at 200°C/5 kg) was 3 cm^3/10 min.

PS/SBR blend, PS/BA 25 nm or 220 nm binary and PS/SBR/BA 220 nm ternary nanocomposites were prepared by water mediated-continuous technique (WM-CT) in a twin-screw extruder, as reported previously in Ref. [17]. For the compounding of the composites a special mixing screw of the corotating ZSK 25 P8 extruder (Werner&Pfleiderer, Stuttgart, Germany) was used. First, BAs particles were dispersed in water at ambient temperature under continuous mechanical stirring for 30 minutes to obtain an aqueous BA slurry, in which the BA content was 30 wt.%. The SBR and/or BA contents in the binary and ternary composites were set for 10 and 3 wt.%, respectively. The PS based composites were compounded at an output rate of 10 kg/h by setting the barrel temperatures between 150 and 190 °C. SBR latex and aqueous BAs slurry were injected into the extruder at a rate of 2 L/h and 1 L/h, respectively, using one (binary composites) or two pumps (ternary composites) of Nemo® Pumpe (Netzsch, Waldkraiburg, Germany).

Injection molding process

The granulated materials were injection molded into standard dumbbell-shaped specimens (160x10x4 mm^3, according to the DIN-ISO-527 standard) by an automatic injection molding machine (Alburg Allrounder 320S, Lossburg, Germany). The barrel temperature of the machine was set at 200°C and that of the mold at 50°C. The injection pressure was kept constant (700 bar), and an injection speed of 55 cm^3/s was selected. The cooling time was 20 s.

Characterization and testing

Morphology detection

The dispersion of BA in the PS nanocomposites was studied by transmission and scanning electron microscopy techniques (TEM and SEM, respectively). TEM measurements were carried out with a Zeiss LEO 912 Omega transmission electron microscopic (Oberkochen, Germany) applying an acceleration voltage of 120 kV. Thin sections (ca. 50 nm) were cut at room temperature with a Diatome diamond knife (Hatfield, PA, USA) using an Ultracut E microtome (Reichert and Jung, Vienna, Austria). The fracture surfaces of injected specimens were subjected to SEM inspection in a Supra™ 40VP SEM (Carl Zeiss GmbH, Oberkochen, Germany). The surface was carbon coated prior to SEM inspection performed at low acceleration voltage.

Mechanical response

Tensile tests were performed on dumbbell-shaped specimens (DIN-ISO-527) on a Zwick 1474 (Ulm, Germany) universal testing machine. Tests were run at room temperature at v=2 mm/min crosshead speed and the related stress-strain curves were registered.

Impact tests were performed on an instrumented impact tester (AFS-MK4 fractoscope of Ceast, Torino, Italy) according to the standard ISO 179. Striker energy of 4 J, acquisition time of 4~8 ms, and incident impact velocity of 2.9 m/s were set. The specimens were rectangular bars (80x10x4 mm^3, length x width x thickness). Measurements were run at ambient temperature on at least six specimens.

Short-time stress relaxation tests were made in three point-bending using the DMA Q800 apparatus (TA Instruments, New Castle, NJ). The strain applied was 0.5 %. The temperature dependence of the stress relaxation response of the PS and its binary and ternary composites was studied in the range from 20 to 60°C, i.e. far below the glass transition temperature (T_g) of PS. Isothermal tests were run on the same specimen in the above temperature range by increasing the temperature stepwise by 10°C and equilibrating the specimen at each temperature for 3 min. During the isothermal tests the duration of the stress relaxation testing was 15 min. The stress relaxation measurement was performed on specimen dimensions of 50 x 10 x 4 mm^3.

3. RESULTS AND DISCUSSION

Morphology

Figure 1a-c compare the fracture surfaces of the PS and PS/BA 220 nm and PS/BA 25 nm composites. SEM picture shows the onset of a rather smooth surface with hints for limited subsurface cracking associated with microductile deformation during PS fracture (cf. figure 1a). One can also recognize that BA 220 nm and BA 25 nm particles were homogeneously dispersed in PS matrix when produced by the WM-CT technique. Secondary cracking due to the nanoscaled dispersed particles causing a dimple pattern is obvious for the composites containing BA 220 nm and BA 25 particles (cf. Figures 1b and 1c). The dimple pattern is more regular for BA 220 (cf. Figure 1b) than for BA 25 (cf. Figure 1c) which suggests that the coarser BA is more uniformly dispersed in the PS matrix than the finer one. This is probably due to the fact that BA 220 has less tendency for agglomeration than BA 25 owing to its smaller specific surface. A characteristic TEM picture taken from the PS/BA 220 confirms the homogeneous distribution of the BA 220 nm particles (cf. Figure 2a). The particle range of BA 220 is in between 100 and 300 nm with a mean value (ca. 190 nm) very close to the referred one in Figure 2a. This suggests that the dispersion of BA in water (cf. section: Materials and preparation of composites) could be maintained during the water-mediated melt compounding followed. Figure 2b shows the TEM image on the dispersion of the SBR particles in the PS matrix. Note that they are in submicron range (particle size less than 600 nm) which is essential for a toughening agent. In case of the ternary composite one can observe that most of BA 220 particles were selectively embedded in the SBR particles (cf. Figure 2c), though a small portion of BA could also be resolved in the PS matrix (not shown here). Attention should be paid to the fact that the particle size range of BA 220, embedded in SBR in the ternary composite, was closely matched with that of BA 220 in the binary system (cf. Figure 2a). Major reason of the selective embedding of BA by SBR is that rubbers can be far higher filled than thermoplastics, even when of amorphous type and similar chemical nature, owing to the large difference between the conformational flexibilities of their chains.

Tensile characteristics

Results of the tensile strength and modulus are given in Figure 3. It is clearly seen that the incorporation of different BA sizes and SBR particles strongly affected the mechanical behavior of PS. By incorporation of BA 25 nm and BA 220 nm particles, the stiffness and strength of the corresponding composites increased compared to the neat PS. It is interesting to note that the particle size of the BAs particles affected the tensile modulus and strength data. For the nanocomposites containing 3 wt.% of BA 25 nm and BA 220 nm particles, the stiffness was improved by approx. 15 % and 7%, respectively, compared to the neat PS. The increase in the tensile modulus

with BA 25 filling is due to its higher specific surface area compared to BA 220 which strongly contributes to the reduction of the mobility of the PS chains in the polymer/filler interphase layers. Similar reported by Starkova et al. [18] for polyamide-66 (PA-66) filled with TiO_2 nanoparticles of various sizes. They observed that the tensile modulus of PA-66 with smaller nanoparticles was greater than with larger ones at the same filler content.

By contrast, adding 10 wt.% SBR particles markedly reduced the tensile strength and modulus. The reduction in the mechanical properties has to be attributed to the softening effect of SBR because there is a large difference in tensile moduli between PS and SBR. The PS/SBR/BA 220 ternary composite exhibited slightly smaller tensile modulus and strength than the PS reference but remained still higher than that of PS/SBR blend. This behavior may be traced to the preferred location of BA particles, being encapsulated in the SBR phase, due to which the reinforcing effect of BA is limited**.**

Impact performance

It has been reported that adding nanoparticles efficiently increases the tensile strength and stiffness, however at cost of the toughness [17]. This is in accordance with our present tensile and impact results (cf. Figures 3 and 4). It can be seen that incorporation of BA 25 nm and BA 220 nm particles was accompanied with a reduction both in the elongation at break and impact energy. By contrast, the SBR domains present in PS prominently enhanced the elongation at break and Charpy impact energy (cf. Figure 4). The Chapy impact strength of PS/SBR became four times higher than that of the reference PS. Additional incorporation of BA 220 into PS/SBR blend reduced, however, both aforementioned parameters. This is obviously due to the BA embedding in the SBR affecting the cavitation behavior of the SBR rubber particles. It has to be mentioned that rubber cavitation is usually the first step in the energy absorbing failure mechanisms of toughened thermoplastic which is followed by combined shear deformation and crazing [19].

Stress relaxation response

Figure 5a and 5b show the traces of the relaxation modulus (Er) as a function of time for the PS, PS/SBR blend, PS binary and ternary composites at the temperature of 20 °C and 60 C°, respectively. It is clear from figure 5a-b in both temperatures investigated that in presence of BAs particles the mobility of PS chains decreases, which resulted in an increase of the relaxation modulus. On the other hand, with increasing temperature the course of the relaxation modulus as a function of time changed for all PS system studied. The relaxation modulus decreased markedly with increasing temperature and time. Note that E_r was strongly enhanced by the incorporation of BA 25 nm. This is in harmony with the tensile test results (increased tensile stiffness and thus relaxation modulus) and confirms the reinforcing effect of the smaller BA particles by contrast to the larger ones (BA 220 nm). The presence of SBR particles caused a reduction in the relaxation modulus. The relaxation modulus of PS/SBR at T = 20 °C and 60 °C after the full relaxation time (i.e. 900 s) was markedly lower than the PS reference. It is interesting to note that the PS/SBR/BA composite showed a higher modulus in the whole time range at all temperatures compared to the PS/SBR binary blend. This is obviously an effect of the BA reinforcement in the SBR phase.

It is well known that viscoelastic behaviors depend on the morphology and the dispersion state of nanoparticles. In order to obtain a deeper insight into the stress relaxation response of the PS systems studied, the elastic and viscoelastic parts of the relaxation modulus have been considered. The relaxation modulus can be treated as consisting of two components: the elastic (E_{r0}, instantaneous, time-independent) and the viscoelastic (E_{rv}, reversible, time-dependent).

$$E_r(t,\varepsilon,T) = E_{r0}(\varepsilon,T) + E_{rv}(t,\varepsilon,T) \quad (1)$$

where ε is the applied strain, T is the temperature and t is the time.

Figure 6 demonstrates the effect of increased temperature on the elastic (E_{r0}) and viscoelastic (E_{rv}) parts of relaxation modulus. One can notice that E_{r0} of the PS/BA composites decreased slowly with increasing temperature. The composite with BA 25 nm exhibited the highest E_{r0} and E_{rv} at the whole evaluated temperature range. This can be attributed to the reinforcing effect of this nanoscale dispersed BA 25 in the PS matrix. This finding is in analogy with the results of Deshmukh et al. [20] reporting that the stiffness of mica filled PVC composite changed markedly with varying particle size. Note that E_{r0} and E_{rv} of the PS ternary composites were always higher than that of the PS/SBR blend. It is also striking that the course of both the E_{r0} and E_{rv} as a function of temperature is quite similar, i.e. the related traces are running more or less parallel to one another. This suggests that the modification with BA and SBR affects the stress relaxation modulus but its change with the temperature is governed by the PS matrix itself. Similar conclusion was drawn for the creep behavior of nanoreinforced PS in our former work [3]. The only exception in this respect is given by the ternary system (PS/SBR/BA) showing a steeper change of the elastic and viscoelastic stress relaxation moduli in function of temperature than all other systems. This should be an effect of BA encapsulation in the SBR phase. Obviously at high temperatures the relaxation of the BA-filled SBR accelerates. The reason behind may be a difference in the thermal expansion of PS and BA-filled SBR assuming that the temperature does not influence the movement of the absorbed PS chains on the BA surface.

In order to describe the stress relaxation behavior of the systems studied the applicability of the inverse Findley power law has been checked. This model was proved to be capable of predicting the nonlinear viscoelastic response. The inverse of the Findley model prediction was already successfully adapted to estimate the stress relaxation behavior of a nanoreinforced PS [21-22]. The inverse of the Findley power law equation is given by:

$$E_{rF} = \left(E_{rF0} + E_{rF1} * t^n\right)^{-1} \quad (2)$$

where the subscript F indicates that the parameters are linked with the Findley power law, n is a constant independent of strain, Er_{F0} is the time-independent relaxation modulus and Er_{F1} is coefficient of the time-dependent term.

The relaxation moduli of the PS, PS/SBR blend, PS binary- and ternary composites were measured at different temperatures and shifted by considering the time temperature superposition (TTS): $a_T = E_r(t, T)/(E(t, T_{ref.})$, where a_T is the shift factor, t is the relaxation time, T and T_{ref} are the actual and

reference temperatures, respectively ($T_{ref.}$ = 30°C was chosen in the present case). It is well resolved that there is a fair agreement between the master curves and those predicted by the inverse Findley equation. The only exception is given again by the PS/SBR/BA ternary system. So, when BA is encapsulated in SBR, may not follow the traditional stress relaxation behavior - especially at high temperatures - due to the highly increased mobility of the SBR chains and to associated void formation. The stress relaxation curves testify that the relaxation modulus is highly influenced by the primary particle size of the BA. Incorporation of BA 25 nm particles increased the modulus compared to the BA 220 nm nanocomposite for the whole estimated time range. The Arrhenius equation was adopted to compute the stress relaxation activation energy (Ea) values. By comparing the activation energies (cf. Figure 7), one may conclude that the Ea increased with decreasing mean particle size of BA. This result suggests that Ea may be sensitive to the primary particle size of the BA. Incorporation of BA 220 nm into the PS/SBR yielded also an increase in Ea that can be traced to the selective encapsulation of BA by the SBR. It has to be underlined here that the Ea values were derived from a single test series, performed on the same specimen, for each composition and thus they may underline a large scatter. Nonetheless, traces in Figure 7 substantiate a good agreement between the master curve and inverse Findley approaches.

4. CONCLUSION

This work examined the effect of boehmite alumina (BA 220 nm and BA 25 nm) fractions in styrene-butadiene rubber (SBR) toughened polystyrene (PS). The BA and SBR was introduced in the PS matrix via water-mediated melt compounding (WM) using a twin-screw extruder. Based on the results the following conclusions can be drawn:

- SEM and TEM results have shown that WM resulted in homogeneous dispersions of both BA and SBR in the binary composites. BA was mostly encapsulated by the SBR in the ternary PS/SBR/BA composites.

- Incorporation of BA enhanced the stiffness, strength and reduced the impact strength of PS. The modulus and strength of the PS/BA 25 composite was markedly higher than that of PS/BA 220. The effect of particle size of BA was best reflected in the tensile mechanical response. The impact resistance and elongation at break of PS was highly enhanced by the addition of SBR rubber but reduced with additional BA 220 nm filling.

- Addition of SBR decreased the relaxation modulus of PS. Conversely, the incorporation of BA particles into the PS/SBR blend resulted in a considerable increase of the elastic and viscoelastic parts of relaxation modulus. This finding was traced to the selective reinforcement of the SBR particles by BA in the PS/SBR/BA 220 ternary system.

- Based on isothermal short-term stress relaxation experiments master curves in form of stress relaxation modulus vs. time were constructed by adapting the time-temperature superposition (TTS) principle. The related master curves of PS binary and ternary composites could be well approximated by the inverse of the Findley power law.

Acknowledgement

This work is connected to the scientific program of the "Development of quality-oriented and harmonized R+D+I strategy and functional model at BME" project, supported by the New Hungary Development Plan (Project ID: TÁMOP-4.2.1/B-09/1/KMR-2010-0002).

References

[1] Sikka M, Cerini LN, Ghosh SS, Winey KI. Melt intercalation of polystyrene in layered silicates. J Polym Sci Part B: Polym Phys 1996; 34: 1443-1449.

[2] Kim TH, Lim ST, Lee CH, Choi HJ, Jhon MS. Preparation and rheological characterization of intercalated polystyrene/organophilic montmorillonite nanocomposite. J Appl Polym Sci 2003; 87: 2106-2112.

[3] Siengchin S, Karger-Kocsis J. Creep behaviour of polystyrene/fluorohectorite micro- and nanocomposites. Macromol Rapid Commun 2006; 27: 2090-2094.

[4] Sohn JI, Lee CH, Lim ST, Kim TH, Choi HJ, Jhon MS. Viscoelasticity and relaxation characteristics of polystyrene/clay nanocomposite. J Mater Sci 2003; 38: 1849-185.

[5] Vuluga Z, Donescu D, Radovici C, Marinache D, Serban S, Vuluga DM, Paven H. The morphology of polystyrene/organoclay nanocomposites obtained by dynamic melt intercalation. Mater Plast 2004; 41: 3-6.

[6] Dazhu C, Haiyang Y, Pingsheng H, Weian Z. Rheological and extrusion behavior of intercalated high-impact polystyrene/organomontmorillonite nanocomposites. Compos Sci Technol 2005; 65: 1593-1600.

[7] Jeong HM, Choi JS, Ahn YT, Kwon KH. Characteristics of polystyrene/organoclay nanocomposites prepared by in-situ polymerization with macroazoinitiator containing poly(dimethylsiloxane) segment. J Appl Polym Sci 2006; 99: 2841-2847.

[8] Yilmazer U, Ozden G. Polystyrene–organoclay nanocomposites prepared by melt intercalation, in situ, and masterbatch methods. Polym Compos 2006; 27: 249-255.

[9] Lim YT, Park OO. Rheological evidence for the microstructure of intercalated polymer/layered silicate nanocomposites. Macromol Rapid Commun 2000; 21: 231-235.

[10] Wang Z, Li G, Peng H, Zhang Z, Wang X. Study on novel antibacterial high-impact polystyrene/TiO2 nanocomposites. J Mater Sci 2005; 40: 6433-6438.

[11] Ma CCM, Chen YJ, Kuan HC. Polystyrene nanocomposite materials: Preparation, morphology, and mechanical, electrical, and thermal properties. J Appl Polym Sci 2005; 98: 2266-2273.

[12] Amr IT, Al-Amer A, Thomas S, Al-Harthi M, Girei SA, Sougrat R, Atieh MA. Effect of acid treated carbon nanotubes on mechanical, rheological and thermal properties of polystyrene nanocomposites. Composites Part B 2011; 42: 1554-1561.

[13] Siengchin S, Karger-Kocsis J. Polystyrene nanocomposite produced by melt compounding with polymer coated magnesium carbonate nanoparticles. J Reinf Plast Compos 2012; 31: 145-152.

[14] Gao X, Qu C, Zhang Q, Peng Y, Fu Q. Brittle-ductile transition and toughening mechanism in POM/TPU/CaCO3 ternary composites. Macromol Mater Eng 2004; 289: 41-48.

[15] Lu M, He B, Wang L, Ge W, Lu Q, Liu Y, Zhang L. Preparation of polystyrene–polyisoprene core–shell nanoparticles for reinforcement of elastomers. Composites Part B 2012; 43: 50-56.

[16] Siengchin S, Karger-Kocsis J. Structure, mechanical and fracture properties of nanoreinforced and HNBR-toughened polyamide-6. J Appl Polym Sci 2012; 123: 897-902.

[17] Siengchin S, Karger-Kocsis J, Thomann R. Nanofilled and/or toughened POM composites produced by water-mediated melt compounding: Structure and mechanical properties. eXPRESS Polymer Letters 2008; 2: 746-756.

[18] Starkova O, Yang J, Zhang Z. Application of time–stress superposition to nonlinear creep of polyamide 66 filled with nanoparticles of various sizes. Compos Sci Technol 2007; 67: 2691-2698.

[19] Karger-Kocsis J. Reinforced polymer blends. In: Paul DR, Bucknall CB, editors. Polymer blends, volume 2. New York: John Wiley & Sons, 2000. P. 395-428.

[20] Deshmukh SP, Rao AC, Gaval VR, Joseph S, Mahanwar PA. Effect of particle size and concentration on mechanical and electrical properties of the mica Filled PVC. J Min & Mater Charact & Eng 2010; 9: 831-844.

[21] Siengchin S, Abraham TN, Karger-Kocsis J. Structure–stress relaxation relationship in polystyrene/fluorohectorite micro- and nanocomposites. Mech Compos Mater 2008; 44: 495-504.

[22] Siengchin S, Karger-Kocsis J. Mechanical and stress relaxation behavior of Santoprene® thermoplastic elastomer/boehmite alumina nanocomposites produced by water-mediated and direct melt compounding. Composites Part A 2010; 41: 768-773.

Figures Captions

Figure 1: SEM pictures from the fracture surfaces of PS (a), PS/BA 220 nm (b) and PS/BA 25 nm (c) composites.

Figure 2: TEM pictures from the thin section of PS/BA 220 nm (a), PS/SBR blend (b) and PS/SBR/BA 220 nm (c) composite.

Note that the SBR particles are not always spherical due to their deformation during molding. The white sections in Fig.2c are owing to cutting-caused voiding.

Bitte 2b und 2c auswechseln – Hinweis bei den jeweiligen Bildern!

Figure 3: Tensile mechanical characteristics of the systems studied.

Figure 4: Elongation at break and impact energy characteristics of the systems studied.

Figure 5: Stress relaxation modulus vs. time traces registered at 20 °C and 60 °C.

Figure 6: Effect of temperature on the elastic (E_{r0}) and viscoelastic (E_{rv}) of relaxation moduli.

Figure 7: Collation of the relaxation modulus master curves and the predicted ones using the inverse Findley power law. Note: master curves were constructed by considering the TTS and selecting $T_{ref.}$ = 30 °C. Ea was calculated by the Arrgenius equation, i.e.: $a_T = E_r(t, T)/(E(t, T_{ref.})$.

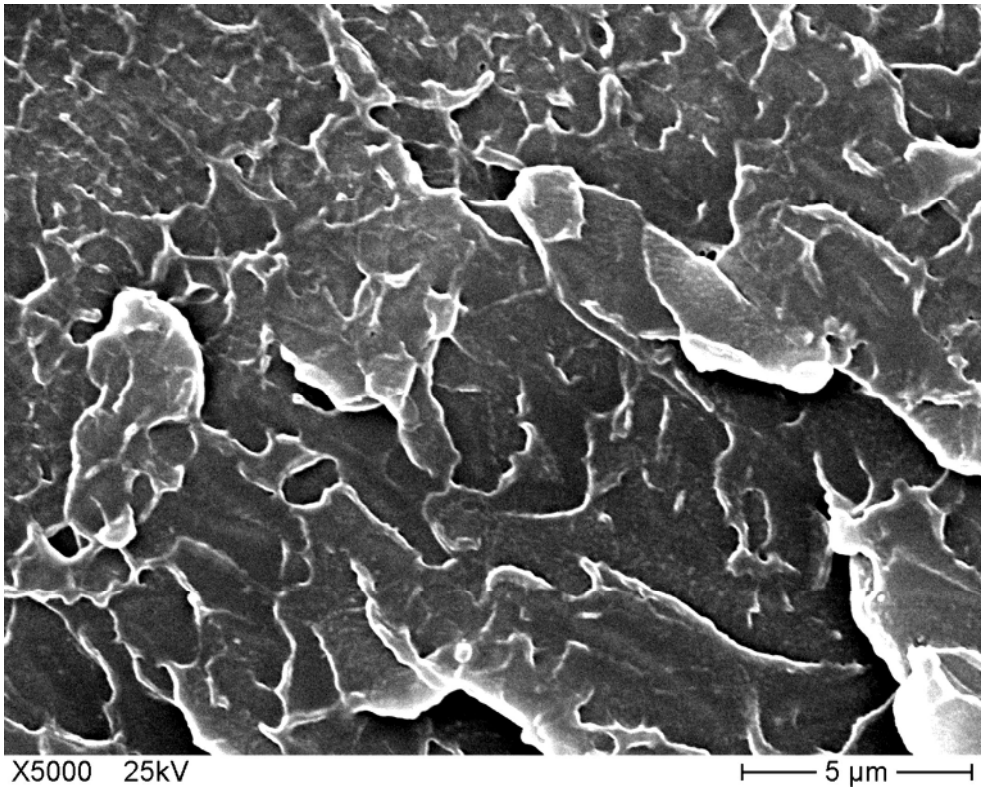

Figure 1a:

Figure 1b:

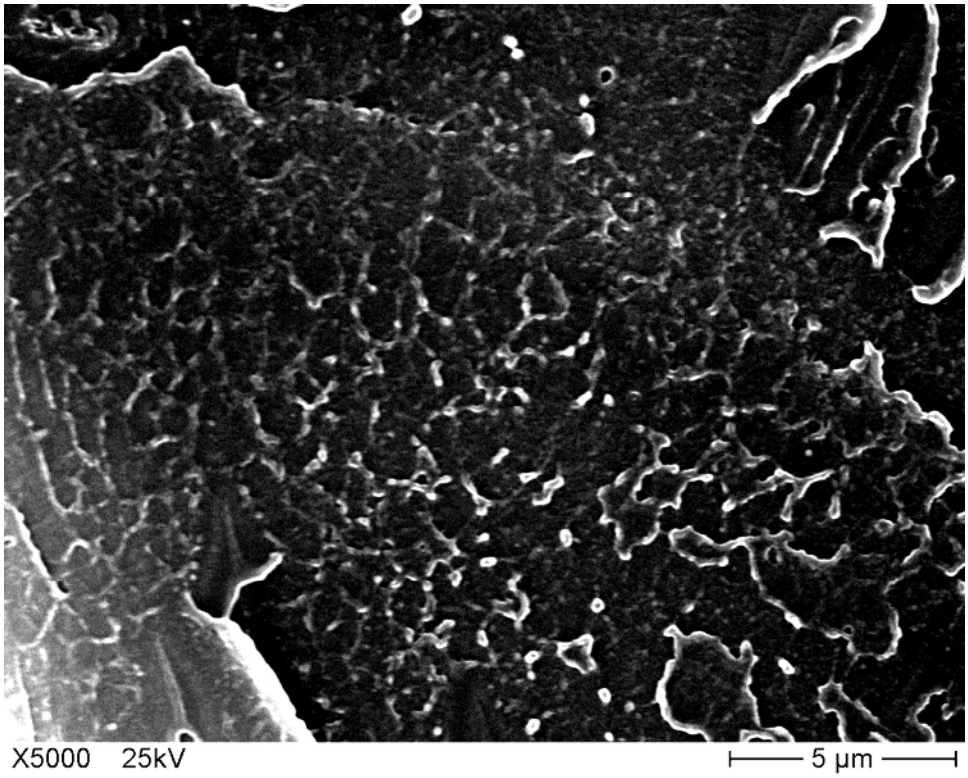

Figure 1c:

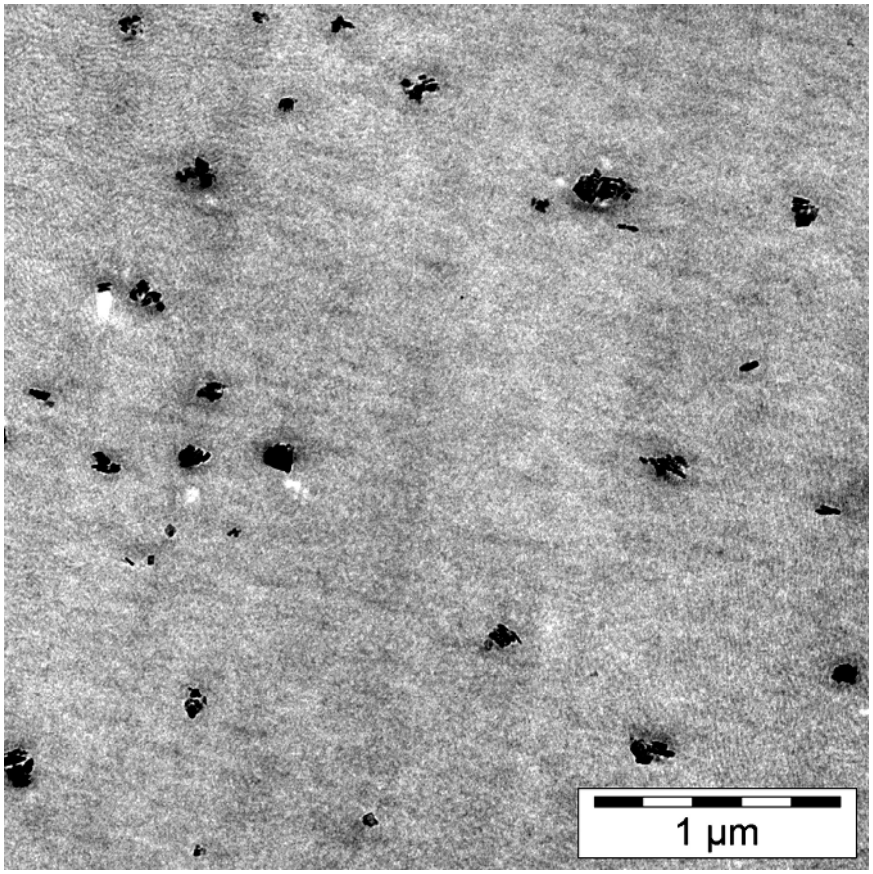

Figure 2a:

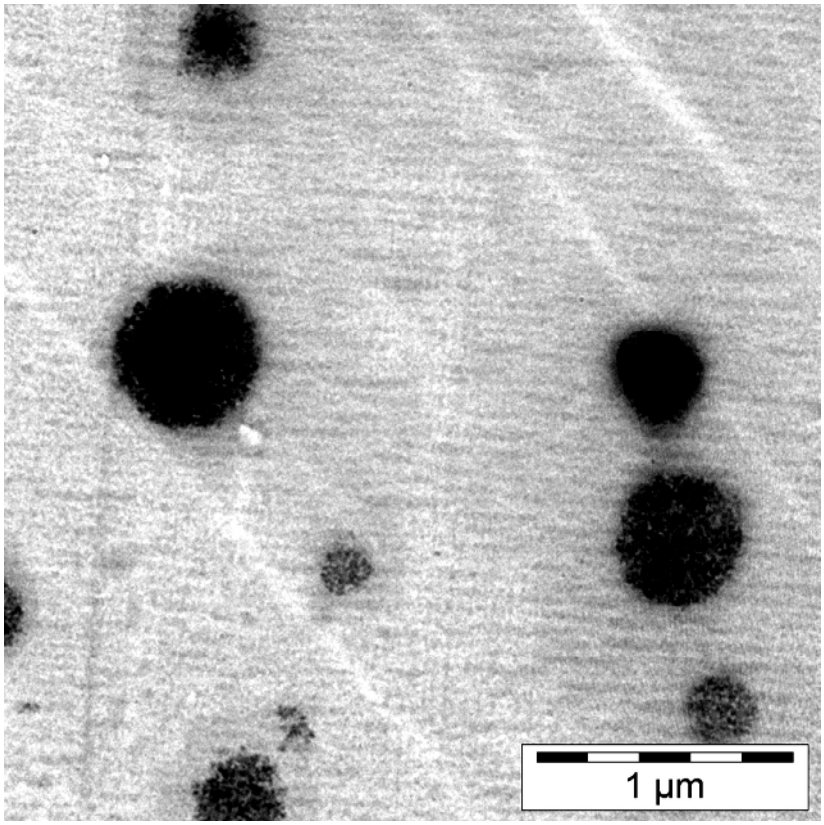

Figure 2b: to replace with 2 Reihe drittes Bild von links - 1 micron scaling

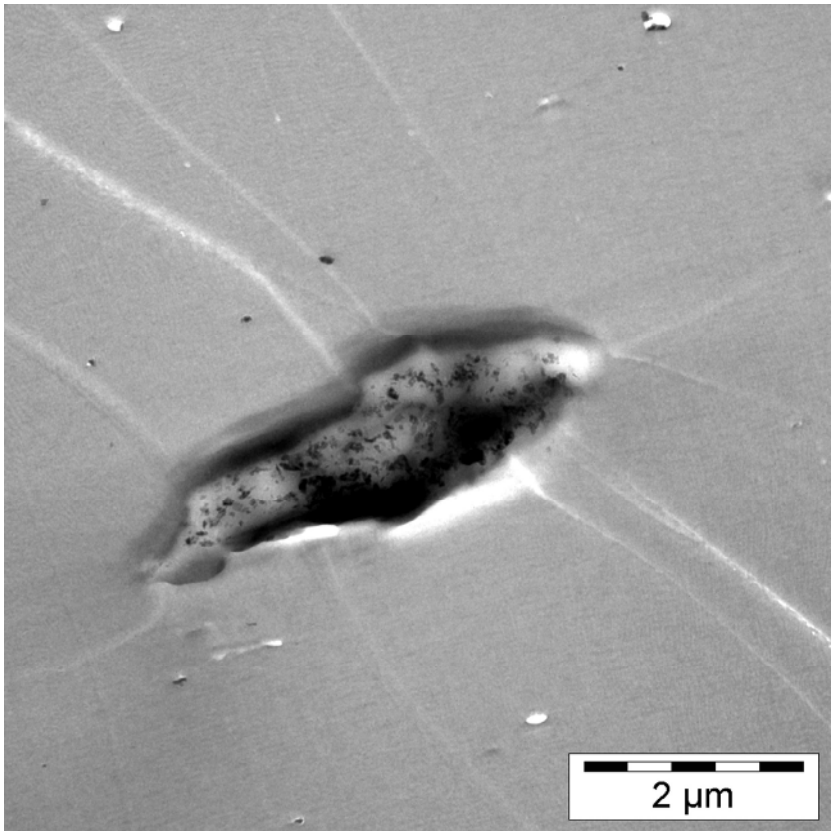

Figure 2c: to replace with TEM picture links oben with a scale of 1 micron

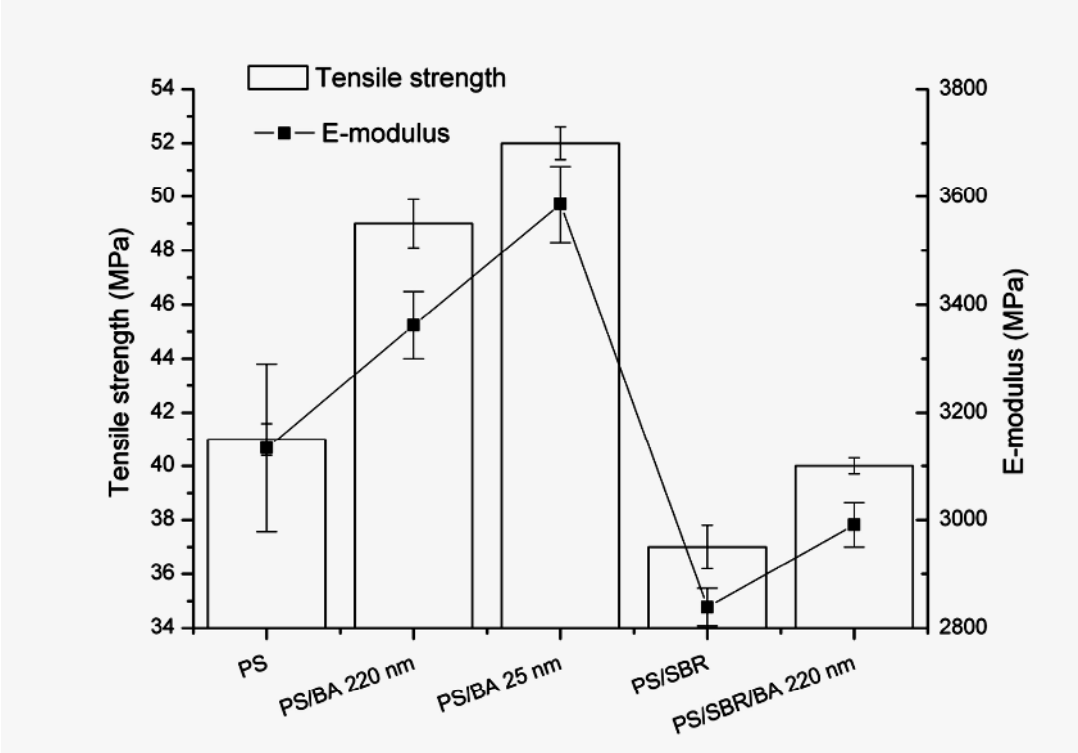

Figure 3:

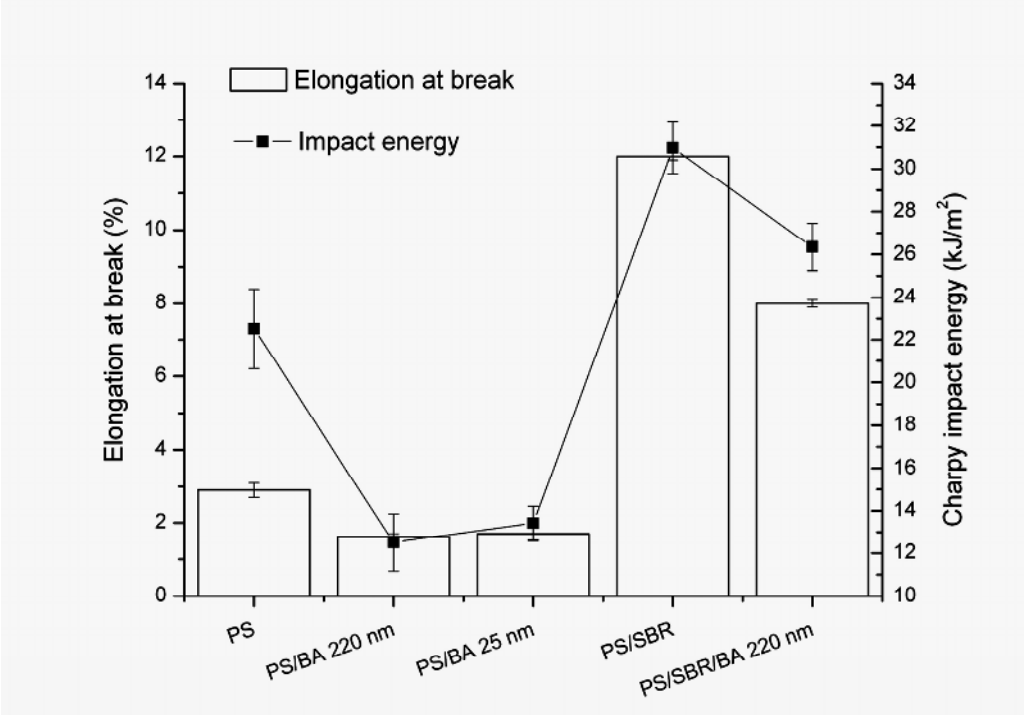

Figure 4:

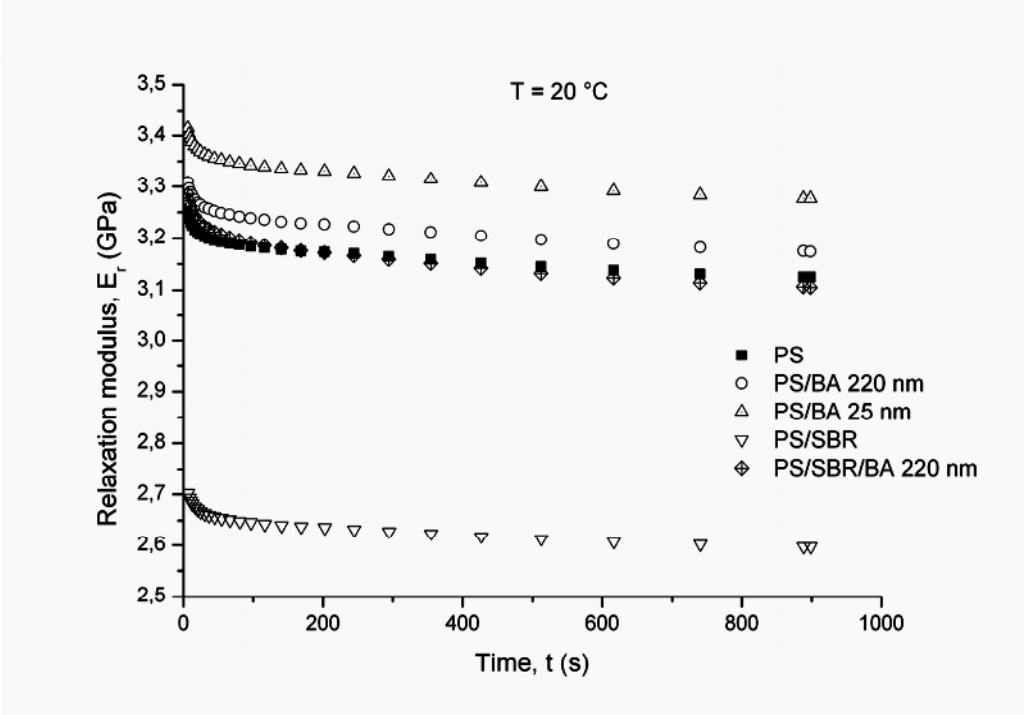

Figure 5a:

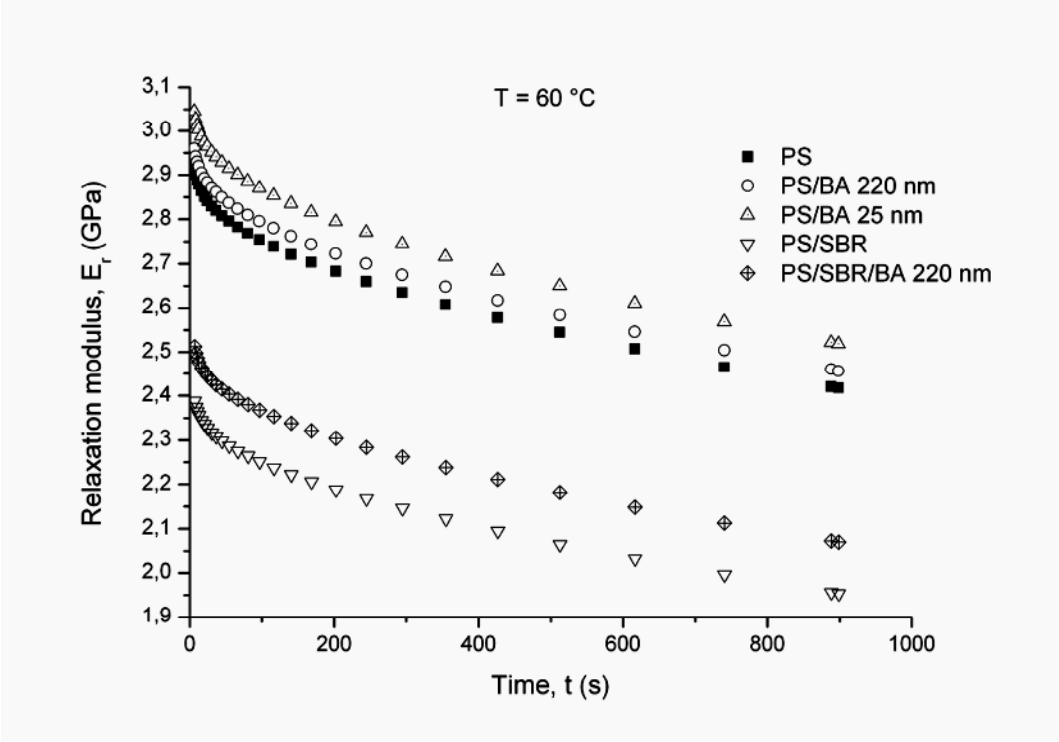

Figure 5b:

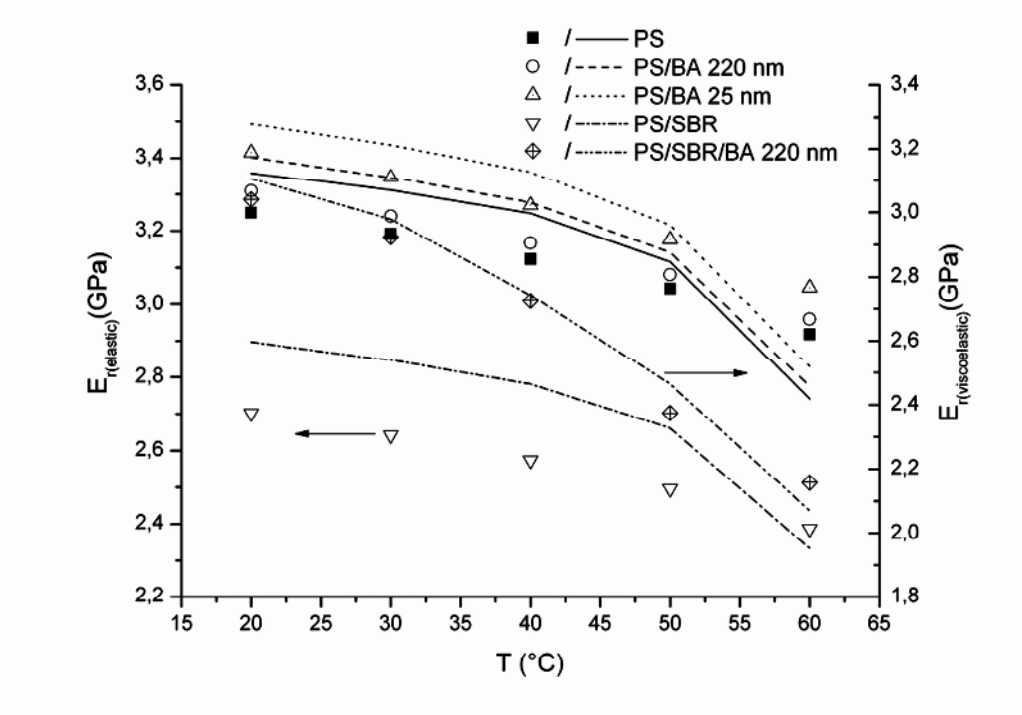

Figure 6:

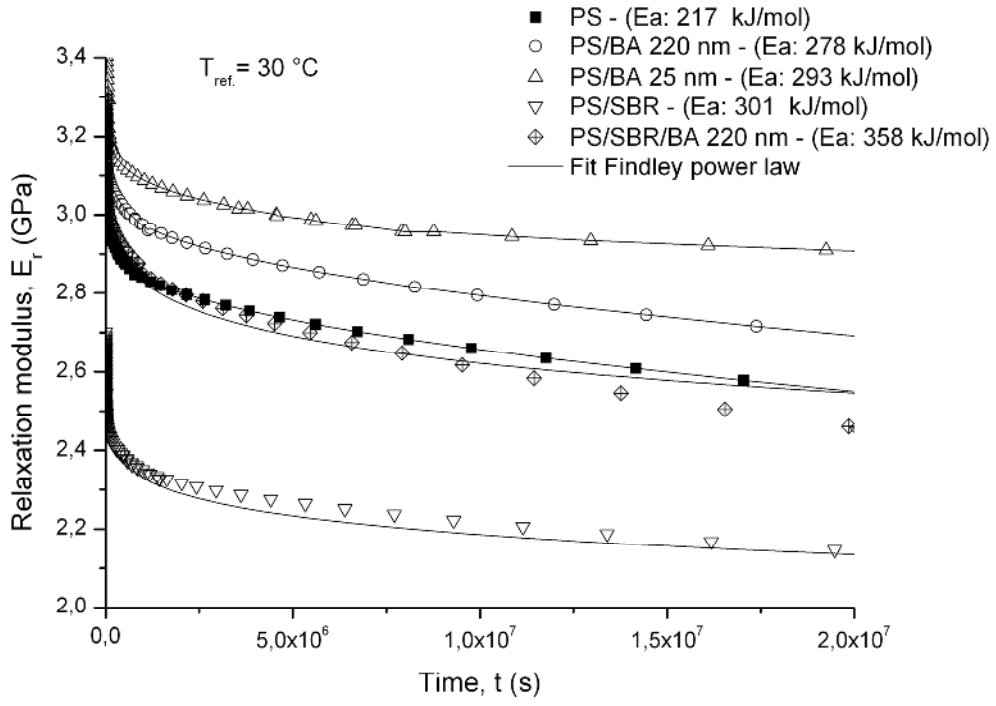

Figure 7: